

High-Accuracy Classification of Radiation Waveforms of Lightning Return Strokes

Ting Wu¹, Daohong Wang¹, Nobuyuki Takagi¹

¹Department of Electrical, Electronic and Computer Engineering, Gifu University, Gifu, Japan

Key Points:

- A machine-learning classifier for negative return strokes is built using a large dataset with 3-D location information
- Both an accuracy and an efficiency of about 98.8% are achieved and the accuracy-efficiency tradeoff can be easily controlled
- Some return strokes and IC discharges produce special waveforms that are fundamentally difficult to classify without 3-D location results

Corresponding author: T. Wu, wu.ting.x4@f.gifu-u.ac.jp

Abstract

A machine-learning classifier for radiation waveforms of negative return strokes (RSs) is built and tested based on the Random Forest classifier using a large dataset consisting of 14,898 negative RSs and 159,277 intracloud (IC) pulses with 3-D location information. Eleven simple parameters including three parameters related with pulse characteristics and eight parameters related with the relative strength of pulses are defined to build the classifier. Two parameters for the evaluation of the classifier performance are also defined, including the classification accuracy, which is the percentage of true RSs in all classified RSs, and the identification efficiency, which is the percentage of correctly classified RSs in all true RSs. The tradeoff between the accuracy and the efficiency is examined and simple methods to tune the tradeoff are developed. The classifier achieved the best overall performance with an accuracy of 98.84% and an efficiency of 98.81%. With the same technique, the classifier for positive RSs is also built and tested using a dataset consisting of 8,700 positive RSs. The classifier has an accuracy of 99.04% and an efficiency of 98.37%. We also demonstrate that our classifiers can be readily used in various lightning location systems. By examining misclassified waveforms, we show evidence that some RSs and IC discharges produce special radiation waveforms that are almost impossible to correctly classify without 3-D location information, resulting in a fundamental difficulty to achieve very high accuracy and efficiency in the classification of lightning radiation waveforms.

Plain Language Summary

Lightning location systems are required to classify return strokes (RSs) from intracloud discharges accurately and efficiently because the RS is the main discharge component that poses direct threats to the human society. In this paper, we report a machine-learning classifier for negative RSs built using a large dataset with accurate 3-D location information. The classifier has an accuracy of 98.84% (98.84% of classified RSs are correct classifications) and an efficiency of 98.81% (98.81% of RSs can be correctly classified). With the same technique, we also built a classifier for positive RSs with similarly high accuracy and efficiency. Our classifiers only require some simple waveform parameters and can be readily used in various national and continental lightning location systems. A sample Python script to use the classifier is provided and readers are encouraged to test the classifier using their own dataset. We also demonstrate that some RSs and intracloud discharges produce abnormal waveforms, so 100% accuracy or efficiency is fundamentally difficult to realize using only waveform information.

1 Introduction

Ground-based lightning location systems (LLSs) are widely used to monitor lightning activities. A prominent feature of ground-based LLSs is that lightning activities in a wide area can be monitored in real time with only a limited number of sensors. Some famous national and continental LLSs include the National Lightning Detection Network (NLDN) covering the continental United States (e.g. Cummins & Murphy, 2009), the European Cooperation for Lightning Detection network (EUCLID) covering the European continent (e.g. Schulz et al., 2016), and the Earth Networks Total Lightning Network (ENTLN) (e.g. Zhu et al., 2022) with the aim of a global coverage.

It is a basic requirement for LLSs to automatically and efficiently classify cloud-to-ground (CG) lightning flashes from intracloud (IC) flashes as the former consist of discharges with direct connections to the ground and thus pose a much larger threat to the human society. The fundamental difference between a CG flash and an IC flash is that a CG flash contains one or more return strokes (RSs), so the classification of CG flashes is basically realized by classifying RSs. Further, it is well known that RSs produce characteristic electric field radiation waveforms that are largely different from those of IC discharges (e.g. Lin et al., 1979), so most LLSs classify RSs based on their waveform characteristics.

62 However, RSs actually can produce radiation waveforms with a variety of special
63 features under some special conditions. For example, some RSs in winter thunderstorms
64 are known to produce abnormal radiation waveforms, some of which could not be correctly
65 classified by LLSs (Wu, Wang, & Takagi, 2021; Wu, Wang, Huang, & Takagi, 2021). It
66 is also well known that RSs striking tall objects produce much narrower radiation waveforms
67 (Pavanello et al., 2007; Zhu et al., 2018). On the other hand, IC discharges include various
68 discharge processes such as narrow bipolar events and recoil leaders, some of which may
69 produce radiation waveforms with certain similar features as RS waveforms. As a result,
70 for most LLSs, it is basically very difficult to achieve a very high classification accuracy
71 of RSs. For example, Zhu et al. (2016) reported that out of 339 RSs in Florida in 2014
72 that were also recorded by the NLDN, 312 (92%) were correctly classified as RSs by the
73 NLDN. Kohlmann et al. (2017) reported that the classification accuracy of EUCLID for
74 RSs were generally around 90% based on ground-truth data in various regions of Europe.
75 For some particular thunderstorms or some special types of discharges, misclassifications
76 by LLSs can be more common. For example, Fleenor et al. (2009) found that 204 out
77 of 376 (54%) of RSs reported by the NLDN during a field campaign in 2005 were actually
78 IC discharges. Leal et al. (2019) found that compact intracloud discharges with estimated
79 peak currents larger than 50 kA were all falsely classified as RSs by both NLDN and ENTLN.
80 Paul et al. (2020) reported that out of 40 RSs detected at the Peissenberg Tower, 12 (30%)
81 were falsely classified as IC discharges.

82 In order to overcome the uncertainties in classifications based only on radiation waveforms,
83 Betz et al. (2004) proposed a pseudo 3-D technique to assist the discrimination of RSs
84 and IC discharges based on the fact that the elevation of IC discharges would have some
85 contributions to the time delay. However, this technique also has some limitations. For
86 example, IC discharges need to have significant elevations, the baseline of the LLS cannot
87 be too long, and lightning discharges first need to be located accurately in 2-D. These
88 limitations prevented the wide implementation of this technique.

89 In recent years, machine-learning techniques have been developing rapidly, and these
90 techniques seem to be promising in significantly increasing the classification accuracy of
91 lightning radiation waveforms. Wang et al. (2020) developed a convolutional neural network
92 to classify radiation waveforms of lightning discharges recorded by the Advanced Direction-time
93 Lightning Detection System in China. They reported an accuracy of over 99%. However,
94 they apparently did not have the height information of lightning discharges and thus could
95 not unambiguously differentiate RSs and IC discharges, so the accuracy remains questionable.
96 Zhu et al. (2021) used the Support Vector Machines (SVM) model to classify CG and
97 IC flashes recorded by the Cordoba Marx Meter Array. The lightning data were in 3-D,
98 so they could employ the discharge height information to build a dataset with accurate
99 discharge types. They reported an overall accuracy of 97%. However, their proposed method
100 requires full waveform information, while most LLSs only retrieve a few parameters of
101 electric field waveforms of lightning discharges, making it somewhat difficult for existing
102 systems to adopt the method.

103 In this paper, we report a simple yet high-accuracy machine-learning technique based
104 on the Random Forest classifier to classify RSs. We will use a large dataset containing
105 about 15,000 negative RSs and many more IC discharges with accurate 3-D location information
106 to train and test the classifier. As will be described in this paper, many of the recorded
107 RSs and IC discharges produced atypical radiation waveforms that were challenging to
108 be correctly classified. However, the accuracy of our classifier is close to 99% demonstrated
109 by evaluations in various respects. Our classifier requires only some simple parameters
110 of lightning radiation waveforms, so it can be readily used by most LLSs.

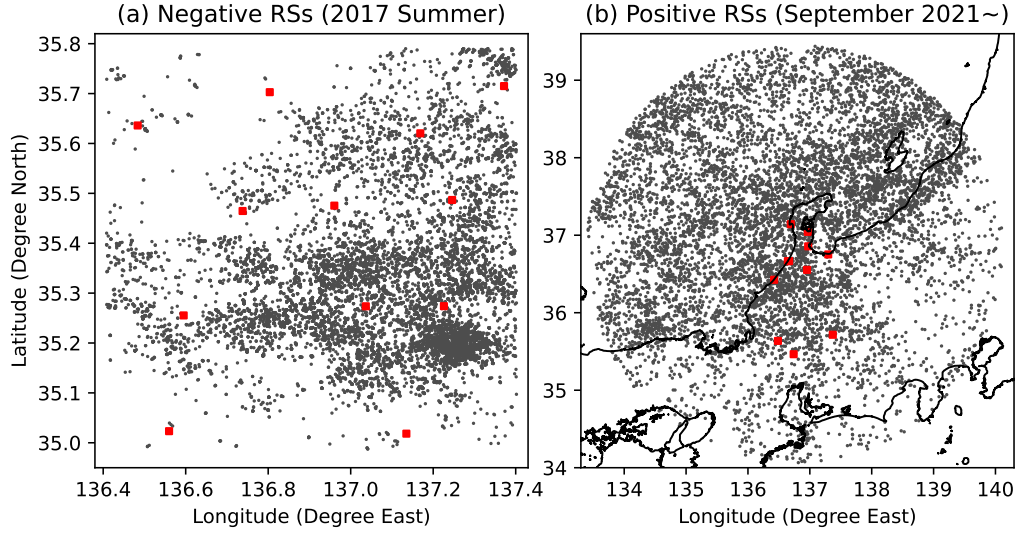


Figure 1. (a) Negative RSs (black dots) observed from July 19 to August 26 in 2017. (b) Positive RSs observed from September 26, 2021 to September 3, 2022. Red squares represent observation sites of FALMA.

111 2 Observation and Data

112 During the summer of 2017, we set up a low-frequency (LF) lightning mapping system
 113 called Fast Antenna Lightning Mapping Array (FALMA) in central Japan. The FALMA
 114 consisted of 12 sites covering an area of about 80×80 km². Locations of these 12 sites
 115 are shown as red squares in Figure 1a. At every site, a fast antenna working in the frequency
 116 band of 500 Hz to 500 kHz was used to receive radiation signals from lightning discharges.
 117 The signals were recorded with a sampling rate of 25 MS/s. As described by Wu et al.
 118 (2018a), thanks to improvements made in both the hardware and the software, we realized
 119 high-quality 3-D lightning mapping with the FALMA. As can be seen from examples of
 120 lightning flashes in Wu et al. (2018a) and Wu et al. (2019), 3-D mapping results of FALMA
 121 have similar quality to those of very-high-frequency (VHF) systems such as the Lightning
 122 Mapping Array (Rison et al., 1999).

123 Data obtained from July 19 to August 26 are used in this study for building and
 124 testing the classifier for negative RSs. All data are reprocessed for this study. The largest
 125 positive pulse (the same polarity as the negative RS, using the atmospheric electricity
 126 sign convention) in each 20-ms window is located in 3-D. Only discharges located in the
 127 region shown in Figure 1a, a 90×90 km² area over the FALMA network, are used in order
 128 to ensure reliable 3-D locating. Pulses with source heights lower than 500 m are treated
 129 as candidates of RSs. Their waveforms are then confirmed manually, and for some ambiguous
 130 pulses, they are further manually located to determine their source heights. In this way,
 131 we can unambiguously determine that the selected pulses are truly RSs. The number
 132 of IC discharges are much larger than that of RSs, so we cannot manually confirm waveforms
 133 of all IC discharges, and we only use pulses with source heights larger than 3000 m as
 134 IC pulses. There are 14,898 pulses confirmed as negative RSs and 159,277 pulses as IC
 135 discharges. Locations of these RSs are shown as black dots in Figure 1a. It should be
 136 noted that we will build a classifier for negative RSs rather than negative CG flashes;
 137 a CG flash consists of at least one RS and also many IC discharges, both of which need
 138 to be correctly classified.

Using the high-quality dataset of 2017 summer, we will establish the technique for building the classifier as will be described in Sections 3.1 to 3.5. Further, using the same technique, we will also build a classifier for positive RSs as will be described in Section 3.6. However, positive RSs in central Japan in summer are quite rare (Wu et al., 2018b). In order to accumulate a large number of positive RSs, we will use the data collected during a long period, from September 26, 2021 to September 3, 2022. During this period, we set up a FALMA network covering a large area for 2-D locating of both summer and winter lightning. Observation sites are shown as red squares in Figure 1b. A total of 8700 positive RSs observed in an area with a radius of 300 km are identified and will be used for building and testing the classifier for positive RSs. Locations of these positive RSs are shown as black dots in Figure 1b. The procedure for the identification of these positive RSs will be further described in Section 3.6.

Our classifiers will be built and tested mainly based on the Random Forest classifier, which is one of the most widely used machine-learning models for classification tasks. A brief comparison will also be made with the SVM classifier, another popular machine-learning model, in Section 3.4.

3 Methods and Results

3.1 Method to Evaluate the Performance of a Classifier

Before building the classifier, first we need to define some parameters as indicators of the performance of a classifier. One obvious parameter to evaluate the performance is the classification accuracy, or simply *accuracy*, that is, the percentage of true RSs in the waveforms classified as RSs. However, only this parameter is apparently not enough, as it is always possible to build a classifier with very strict criteria so that it only identifies very typical RS waveforms. Another important parameter is the identification efficiency, or simply *efficiency*, that is, the percentage of correctly classified RSs in all RSs.

Suppose the number of RSs is N_R , and the number of IC discharges is N_I . Of the N_R RSs, N_{Rc} are correctly classified (the subscript c stands for “correct”), and the remaining $N_R - N_{Rc}$ are misclassified as IC discharges. Of the N_I IC discharges, N_{Ic} are correctly classified, and the remaining $N_I - N_{Ic}$ are misclassified as RSs. The accuracy and the efficiency are defined as follows.

$$Accuracy = \frac{N_{Rc}}{N_{Rc} + (N_I - N_{Ic})} \quad (1)$$

$$Efficiency = \frac{N_{Rc}}{N_R} \quad (2)$$

During the process to build the classifier, we will experiment and tune various parameters of the classifier to make the accuracy and the efficiency as high as possible.

Normally a dataset is split into a larger training set and a smaller test set, with the training set used to train a classifier and the test set used to test or evaluate the performance of the classifier. In this study, we use an improved approach. All RS and IC data are combined, shuffled and then divided into five equal parts. Each part is in turn used as the test set and the remaining four parts combined are used as the training set. In this way, a classifier is built and tested for five times and five results of accuracy and efficiency are calculated. The average values of five tests will be used as the final results. In this way, we can avoid any random biases in the test set. Moreover, as will be described in Section 4, in this way all data can be tested and we can find as many atypical waveforms as possible that are difficult to be correctly classified.

182

3.2 Waveform Parameterization

183

184

185

186

187

188

189

190

We will define some waveform parameters to be used for building the classifier. First we describe the procedure to calculate waveform parameters based on multiple-site records. As waveforms recorded at a close distance contain the electrostatic and induction field components (e.g. Thottappillil et al., 1997) that may significantly distort the waveforms, observation sites within 40 km from a discharge are first excluded. Waveforms recorded by the remaining sites are used to calculate the parameters, and for each parameter, the median value of the results calculated based on these sites are used as the final result of the parameter for the discharge.

191

3.2.1 Parameters Related with Pulse Characteristics

192

193

194

First we define three basic parameters related with pulse characteristics. Definitions of these parameters are illustrated using an RS pulse in Figure 2a and an IC pulse in Figure 2b (blue parameters).

195

196

197

1. T_{rise} : The rise time of a pulse (10% to peak).
2. T_{fall} : The fall time of a pulse (peak to zero).
3. T_{half} : The pulse width at the half maximum.

198

199

200

201

202

203

204

205

206

With only these three basic parameters, we trained and tested the Random Forest classifier using the negative RS and IC dataset obtained in 2017 summer. As described in Section 3.1, the dataset is divided into five parts and each part in turn is used as the test set, so the classifier is trained and tested for five times. The accuracy ranges from 72.25% to 73.57% with an average of 72.82%, and the efficiency ranges from 70.80% to 72.81% with an average of 71.59%. We also tried to add two related parameters, including the pulse width, which is the sum of the rise time and fall time, and the ratio of fall time to rise time, but the result has little difference (the average accuracy is 72.17% and the average efficiency is 70.86%).

207

208

Indeed, with only these basic pulse parameters, it is difficult to accurately classify RSs.

209

3.2.2 Parameters Related with Relative Strength

210

211

212

An important feature of the RS waveform is that pulses right before and after an RS pulse is usually much weaker. The following parameters are defined to employ this feature. These parameters are also illustrated in Figures 2a and 2b.

213

214

215

216

217

218

219

1. R_{bp1} : The ratio of A_0 to A_{bp1} , in which A_0 is the peak amplitude of the target pulse, and A_{bp1} is the maximum amplitude of pulses right before the target pulse (from $-100 \mu\text{s}$ to 10% peak) as illustrated in Figure 2. The subscript b stands for “before”, and the subscript p stands for “positive”.
2. R_{bn1} , R_{bp2} , R_{bn2} , R_{ap1} , R_{an1} , R_{ap2} , R_{an2} : These parameters are defined in the same way as R_{bp1} , also illustrated in Figure 2. Note that the subscript a stands for “after”, and the subscript n stands for “negative”.

220

221

222

223

224

The three parameters defined in Section 3.2.1 along with the eight new parameters defined above are used to train the Random Forest classifier. The accuracy of five tests ranges from 98.86% to 99.32% with an average of 99.02%, and the efficiency ranges from 98.02% to 98.66% with an average of 98.34%. It is clear that these new parameters representing the relative strength are very effective in the classification of RSs.

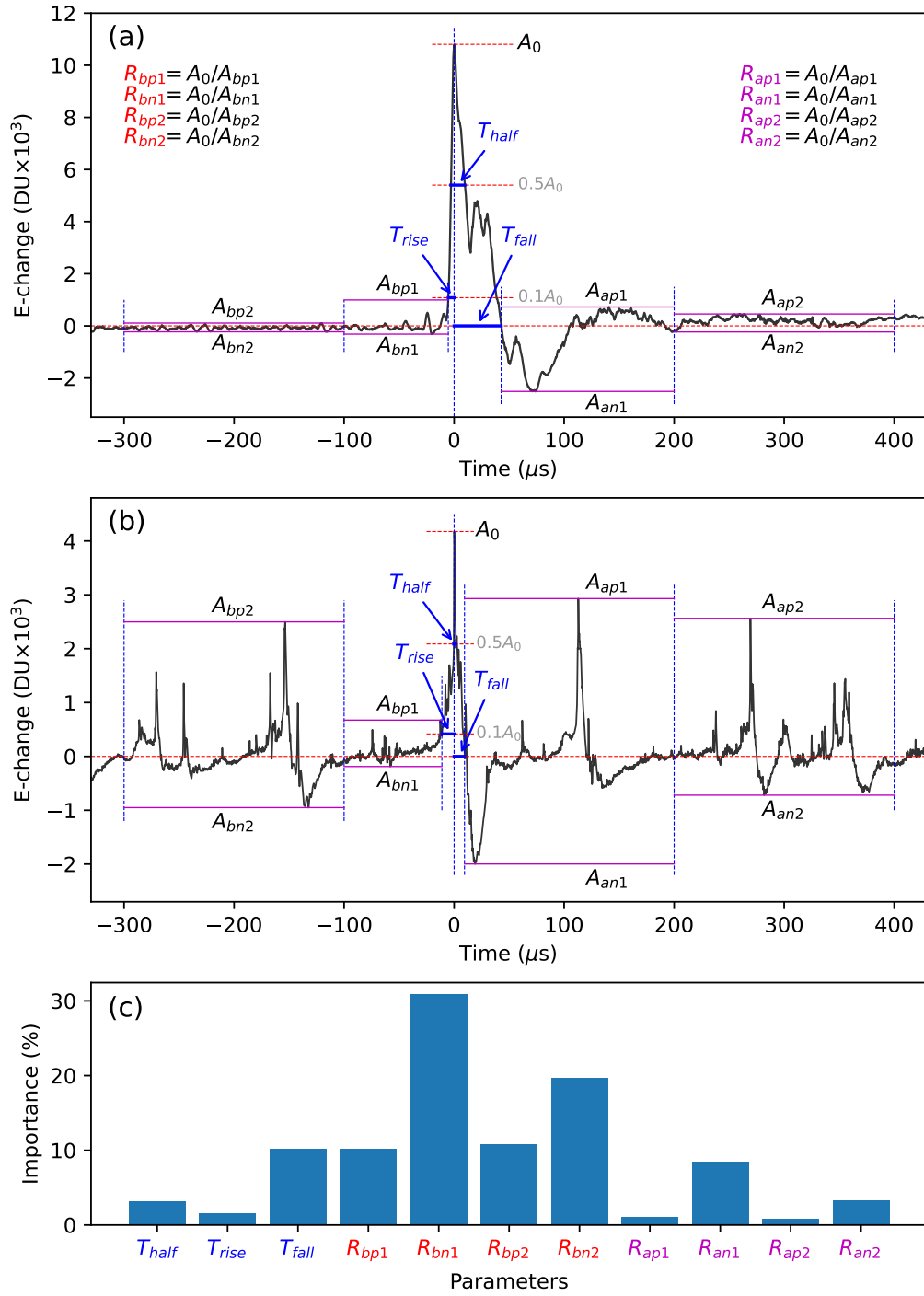


Figure 2. Illustration of waveform parameters using (a) an RS pulse and (b) an IC pulse. (c) Relative importance of waveform parameters.

225

3.2.3 Parameter Importance

226

227

228

229

230

231

232

233

234

235

The Random Forest classifier outputs a value indicating the relative importance of each parameter in contributing to the performance, from which we can evaluate the effectiveness of each parameter in the classification of RSs. The results are shown in Figure 2c. Values of the importance of all parameters combined equal to 1. We can see that parameters related with the pulse strength relative to previous pulses (red parameters in Figure 2) are generally more important than other parameters. This is easy to understand as an RS pulse is preceded by leader pulses which are usually much weaker than the RS pulse. By contrary, an IC pulse is usually preceded by other IC pulses with comparable amplitudes. Therefore, parameters related with the relative strength are very effective in the classification of RSs.

236

237

238

239

We can also see that parameters related with pulse characteristics (blue parameters) have relatively low importance, which is why the classifier performance is very poor with only these parameters as described in Section 3.2.1. It also indicates that traditional RS classification methods based on pulse characteristics are not very reliable.

240

3.3 Tradeoff Between Accuracy and Efficiency

241

242

243

244

245

246

247

From the above result, we can see one feature of the classifier is that the accuracy is always higher than the efficiency. It is obvious that increasing the efficiency usually implies decreasing the accuracy. However, it is desirable if we can control the tradeoff between the accuracy and the efficiency. For example, in some situations, it may be required to identify as many RSs as possible, so a high efficiency is essential while a low accuracy is tolerable. Next we will investigate two factors that influence the tradeoff between the accuracy and the efficiency.

248

3.3.1 Influence of Sample Size Imbalance

249

250

251

252

253

254

One reason for the higher accuracy in the classifier built in the previous section is a much larger sample of IC discharges compared with the sample of RSs. With such a biased dataset, the classifier is more likely to misclassify RSs, as also noted by Zhu et al. (2021). We can simply duplicate the sample of RSs to make the classifier identify more RSs, though at the cost of more misclassifications of IC discharges. Note that the duplication should only be made for the training set.

255

256

257

258

259

260

261

262

263

264

265

With the original dataset, 247 of 14,898 RSs (1.7%) are misclassified, but only 145 of 159,277 IC pulses (0.091%) are misclassified. If we duplicate the dataset of RSs in the training set, the number of misclassified IC pulses increases to 162 while the number of misclassified RSs decreases to 199. We tried to make more duplications and tested the classifier, and the results of the accuracy and the efficiency are shown in Figure 3a. With one duplication of the RS training set, the accuracy decreases from 99.02% to 98.91% but the efficiency increases from 98.34% to 98.66%. With two duplications, the accuracy decreases to 98.84% but the efficiency increases to 98.76%, very close to the accuracy. With further duplications, we can see that both the accuracy and the efficiency are generally very similar, changing between 98.75% and 98.85%, indicating that the sample size imbalance does not have a significant effect any more.

266

267

268

269

270

If we use the average value of the accuracy and the efficiency as the indicator of the overall performance of a classifier, we can see from Figure 3a that with four duplications of the RS training set, the classifier has the highest performance with an accuracy of 98.84% and an efficiency of 98.81%. We treat this as the best performance of the classifier for negative RSs and this classifier will be used for further evaluations in the following section.

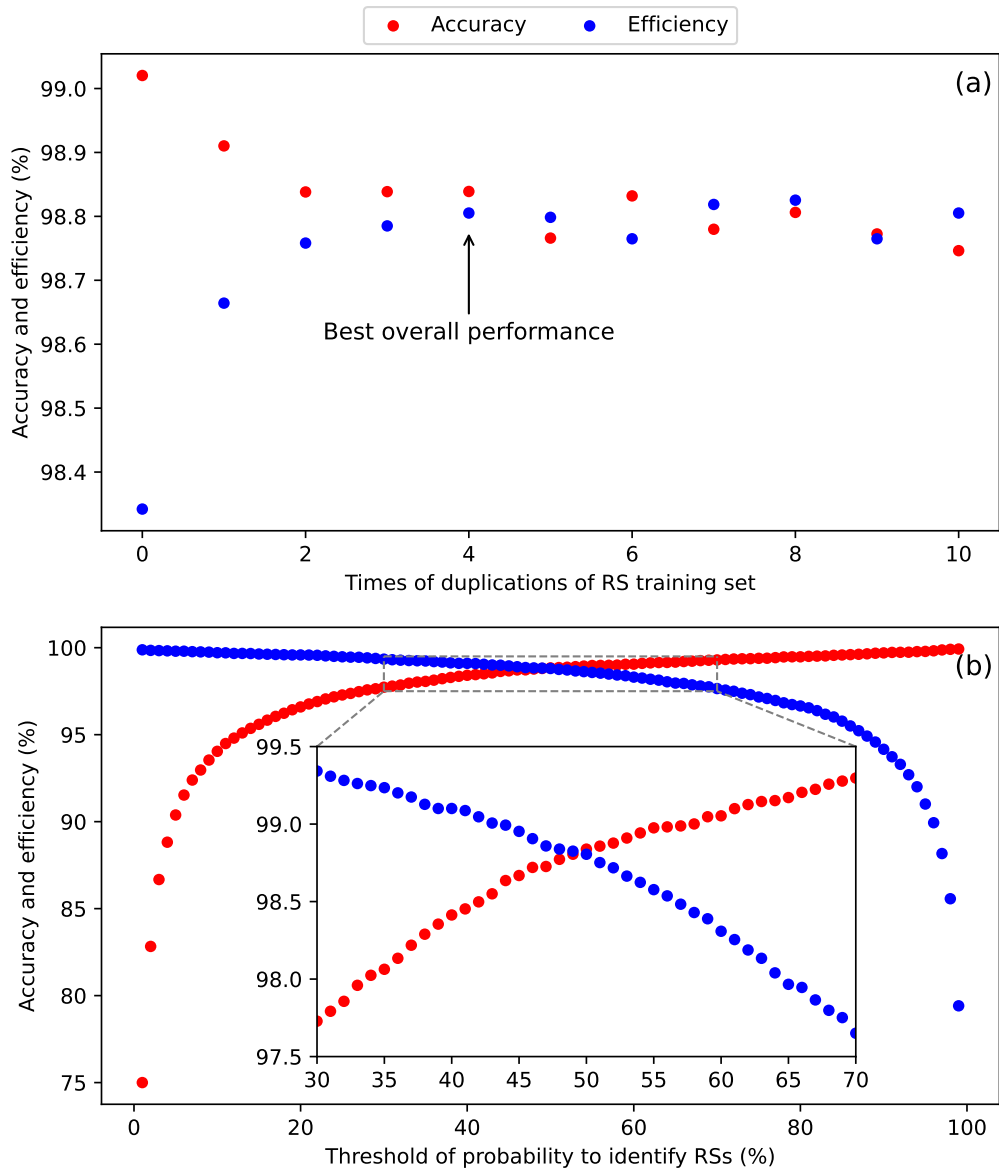


Figure 3. Variations of the accuracy and the efficiency with (a) different times of duplications of RS training set and (b) different thresholds of probability to classify RSs.

Table 1. Comparison of the Random Forest classifier and the SVM classifier

Eleven Parameters (Section 3.2.2)			
Classifier	Accuracy (%)	Efficiency (%)	Time Cost (seconds)
Random Forest	99.02	98.34	20
SVM	98.43	97.42	96
Duplicating RS Training Set (Section 3.3.1)			
Classifier	Accuracy (%)	Efficiency (%)	Time Cost (seconds)
Random Forest	98.84	98.81	28
SVM	97.98	98.09	108

271 3.3.2 Influence of Probability Thresholds

272 When classifying a pulse, the Random Forest classifier can output the probability
 273 that the pulse is a true RS. By default, the classifier determines a pulse as an RS when
 274 the probability is larger than 50%. By changing the probability threshold, we can conveniently
 275 tune the accuracy-efficiency tradeoff.

276 Figure 3b shows variations of the accuracy and the efficiency related with the probability
 277 threshold. We can see that as the probability threshold increases, the accuracy increases
 278 while the efficiency decreases. This is easy to understand; a higher probability threshold
 279 represents stricter criteria to classify RSs, so naturally the identified RSs are more likely
 280 true RSs (higher accuracy), but at the same time fewer RSs can be identified (lower efficiency).
 281 In practice, when using the classifier we can set a customized probability threshold that
 282 fits the specific requirements of an application to achieve desired accuracy or efficiency.

283 3.4 Comparison of Different Machine-learning Models

284 Apart from the Random Forest classifier, another popular machine-learning model
 285 for classification is the SVM classifier, which was used by Zhu et al. (2021) for the classification
 286 of lightning pulses. Here we make a brief comparison of the Random Forest and the SVM
 287 classifiers. First we use the scheme described in Section 3.2.2 (using 11 parameters illustrated
 288 in Figure 2) to train the classifiers, and the results are shown in Table 3.4 (upper part).
 289 We can see the SVM classifier has slightly lower accuracy and efficiency than the Random
 290 Forest classifier. Further, we use the scheme described in Section 3.3.1 (duplicating the
 291 RS training dataset) to train the classifiers, and again, the SVM classifier has slightly
 292 lower accuracy and efficiency. Another difference is in the time needed to train a classifier;
 293 it takes less than 30 seconds to train an Random Forest classifier while the time needed
 294 to train an SVM classifier is around 100 seconds. A significantly shorter time to build
 295 a classifier is potentially very useful as it would be more convenient to experiment various
 296 combinations of parameters in order to boost the performance of the classifier.

297 3.5 Testing Using Remote Lightning Discharges

298 Lightning discharges used for training and evaluating classifiers described above
 299 are all very close to most of FALMA sites in order to ensure the 3-D location accuracy.
 300 However, many LLSs, especially national and continental LLSs, have long baselines of
 301 a few hundred kilometers, so lightning discharges observed by these systems are generally
 302 very far away from most observation sites. Therefore, it is desirable to evaluate the performance
 303 of a classifier for remote lightning discharges.

304 We use lightning discharges located more than 150 km away from the center of the
 305 FALMA network in 2017 summer (the origin in Figure 1a) for this investigation. At such
 306 a large distance, only a small number of discharges can be located with sufficient accuracy,
 307 and we can only make 2-D locating, so we cannot classify RSs using the height information.
 308 Therefore, we manually inspected waveforms of all located events and determine their
 309 types.

310 There are a total of 594 located pulses. The classifier described in Section 3.3.1 (the
 311 training set duplicated for four times) are used to classify these pulses. A total of 361
 312 pulses were classified as RSs, and there was no clear misclassification. The remaining 233
 313 pulses were classified as IC discharges, and four of them were likely RSs. However, it should
 314 be noted that as there is no height information for these pulses, it is sometimes difficult
 315 to determine the true discharge type, so it is possible that there were actually more misclassifications.
 316 Assuming there are only four RSs misclassified as IC discharges, from Equations 1 and
 317 2, we can get an accuracy of 100% and an efficiency of 98.9%. Note that when detecting
 318 remote lightning discharges, as in the case of long-baseline LLSs, only a small portion
 319 of IC discharges that are relatively strong can be located, so the chance of misclassifying
 320 an IC pulse as an RS is relatively low, which may be one reason for the 100% accuracy
 321 in this evaluation.

322 The above results demonstrated that our classifier also has good performance when
 323 classifying remote RSs, so the classifier can also be used in long-baseline LLSs.

324 **3.6 Classification of Positive Return Strokes**

325 The methods described above can also be used to build a classifier for the classification
 326 of positive RSs. However, positive CG flashes are very rare in summer thunderstorms
 327 in central Japan. As reported by Wu et al. (2018b), only 46 positive CG flashes consisting
 328 of 53 positive RSs were observed and could be located in 3-D during the summer observation
 329 of 2017. Therefore, here we also include the data obtained in other periods. First we use
 330 the 690 positive RSs observed during the winter of 2018 (Wu et al., 2022) to build a preliminary
 331 classifier for the identification of positive RSs. Then we use this classifier to search the
 332 data recorded in about one year from September of 2021 for possible positive RSs. As
 333 described in Section 2, during this period, we set up a FALMA network with long baselines
 334 for 2-D locating of both summer and winter lightning. Waveforms of the identified positive
 335 RSs by the preliminary classifier are manually confirmed to exclude obvious false classifications.
 336 Indeed, the preliminary classifier identified many pulses that were clearly IC pulses and
 337 we painstakingly excluded all apparent IC pulses by manual inspections. In this way, we
 338 collected the data of 8700 positive RSs, locations of which are shown in Figure 1b. Note
 339 that there is no height information for these positive RSs, so this dataset is not as accurate
 340 as the negative RS dataset in 2017 summer used in previous sections.

341 For IC data, we also use the data of summer observation of 2017 as these data have
 342 accurate 3-D location results. However, different from the IC dataset for the negative
 343 RS classifier, IC pulses for building positive RS classifier should have the same polarity
 344 as positive RSs. So we located IC pulses having the same polarity as positive RSs and
 345 selected those with heights larger than 3 km, the same treatment as that in building the
 346 negative RS classifier. On the other hand, as the size of positive RS dataset is relatively
 347 small, we do not need too many IC data, so for simplicity, we only located one IC pulse
 348 in every 50-ms window. Finally, we collected a total of 113,922 IC pulses.

349 Using these datasets, and with the same scheme for building negative RS classifier
 350 described in Section 3.3.1, we built and tested the classifier for positive RSs. It is found
 351 that with the RS training set duplicated for one time, the classifier has the best overall
 352 performance. It has an accuracy of 99.04% and an efficiency of 98.37%, generally similar
 353 to the performance of the negative RS classifier. This result demonstrated that as long

354 as there are enough data of positive RSs, we can also build a high-accuracy classifier for
 355 positive RSs in the same way as building the negative RS classifier.

356 Although the dataset of positive RSs does not have 3-D location information and
 357 thus is not as accurate as the negative RS dataset, as positive RSs are much rarer than
 358 negative RSs and it is very difficult to collect a large and reliable sample, we believe our
 359 classifier is very valuable for future observations and researches. Moreover, as all waveforms
 360 of identified positive RSs have been manually confirmed, the classifier likely has an accuracy
 361 similar to that of the manual classification.

362 4 Atypical Intracloud and Return Stroke Waveforms

363 As described in Section 3.1, the whole dataset of 2017 summer is divided into five
 364 parts, with each part in turn used as the testing set and the remaining four parts combined
 365 used as the training set. In this way, all pulses can be tested and we can identify as many
 366 pulses as possible that are potentially difficult to classify. Using the classifier built in Section 3.3.1
 367 with the RS training set duplicated for four times, all pulses are classified. Of the 14,898
 368 RSs, 178 were misclassified as IC discharges, and of the 159,277 IC pulses, 173 were misclassified
 369 as RSs. Waveform figures of all these misclassified pulses are provided in the data repository.

370 There are several common reasons for misclassifications of RS pulses as IC pulses.
 371 Waveforms of four examples are shown in Figures 4a-d, all of which are misclassified as
 372 IC discharges and whose source heights have been confirmed to be close to the ground.
 373 First, it is well known that RSs striking tall grounded objects usually produce very narrow
 374 pulses (Araki et al., 2018; Cai et al., 2022; Pavanello et al., 2007; Zhu et al., 2018), making
 375 it easy to misclassify them as IC discharges. One example is shown in Figure 4a. This
 376 pulse is located near a transmission tower, and its pulse width is only about 6 μ s, indicating
 377 that it is likely produced by an RS striking the tower. Second, two RSs sometimes occur
 378 sequentially with a very small time difference of a few tens of microseconds, and if the
 379 second RS has a larger peak than the first one, the second RS may be misclassified as
 380 an IC pulse. One example is shown in Figure 4b. Such RSs are likely the so-called “multiple-termination
 381 strokes” (Kong et al., 2009; Sun et al., 2016) or “forked strokes” (Ballarotti et al., 2005),
 382 with two RSs induced by two branches of the same leader. Third, an RS may occur almost
 383 simultaneously with IC discharges of other lightning flashes, resulting in a peculiar waveform
 384 and thus misclassified as an IC discharge. One example is shown in Figure 4c. While the
 385 positive pulse is confirmed to be produced by an RS, the two negative pulses labeled as
 386 “IC” are produced by IC discharges in an independent lightning flash and are located about
 387 87 km away from the RS. The resultant waveform appears to be abnormal and is difficult
 388 to be identified as an RS. Finally, some RSs apparently produce waveforms that are largely
 389 different from typical RS waveforms but the reason is not yet clear. One example is shown
 390 in Figure 4d. The pulse has a rise time of about 18 μ s while its fall time is only about
 391 9 μ s.

392 Another example of an RS producing abnormal waveform is shown in Figure 5 along
 393 with location results of the preceding leader. This RS is a subsequent RS. We can see
 394 from the location results in Figure 5a a dart leader with a speed of about 4×10^6 m/s
 395 preceding the RS, and the RS is located very close to the ground as indicated by the cross
 396 sign. From Figure 5c, we can see details of the RS waveform. It contains two peaks with
 397 the second peak much larger than the first one, resulting in a much larger rise time than
 398 the fall time. Without the 3-D location results, it is very difficult to determine that the
 399 waveform is produced by an RS.

400 The major reason for IC discharges misclassified as RSs is that waveforms of some
 401 IC discharges have some similar features as those of RSs. Four examples are shown in
 402 Figures 4e-h. All of these waveforms appear very similar to those of RSs. However, their
 403 source heights range from 5.9 to 15.1 km, indicating that they are produced by IC discharges.

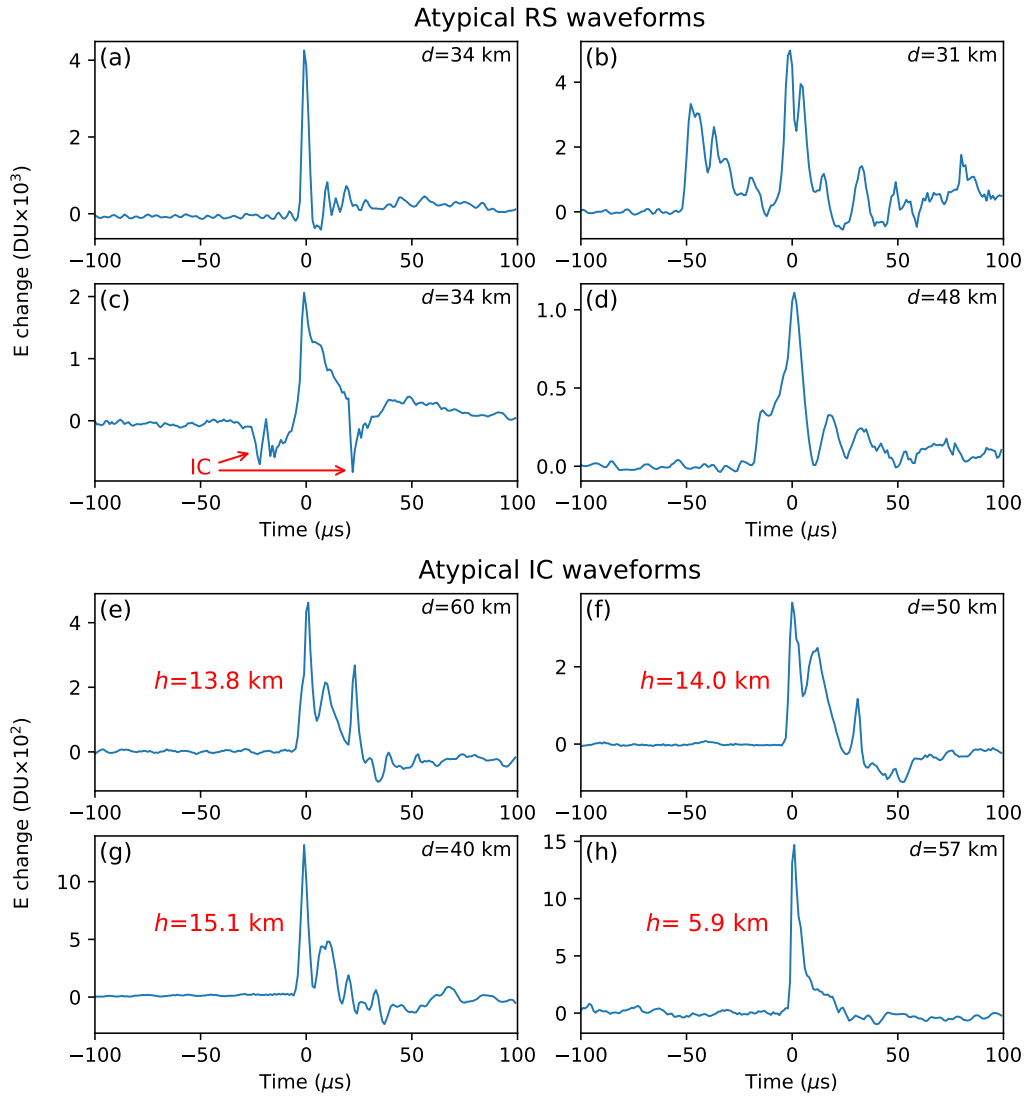


Figure 4. (a)-(d) Atypical E-change waveforms produced by RSs but misclassified as IC discharges. (e)-(h) Atypical E-change waveforms produced by IC discharges but misclassified as RSs. The value of d represents the distance between the discharge and the observation site recording the waveform. The value of h represents the source height of the IC discharge.

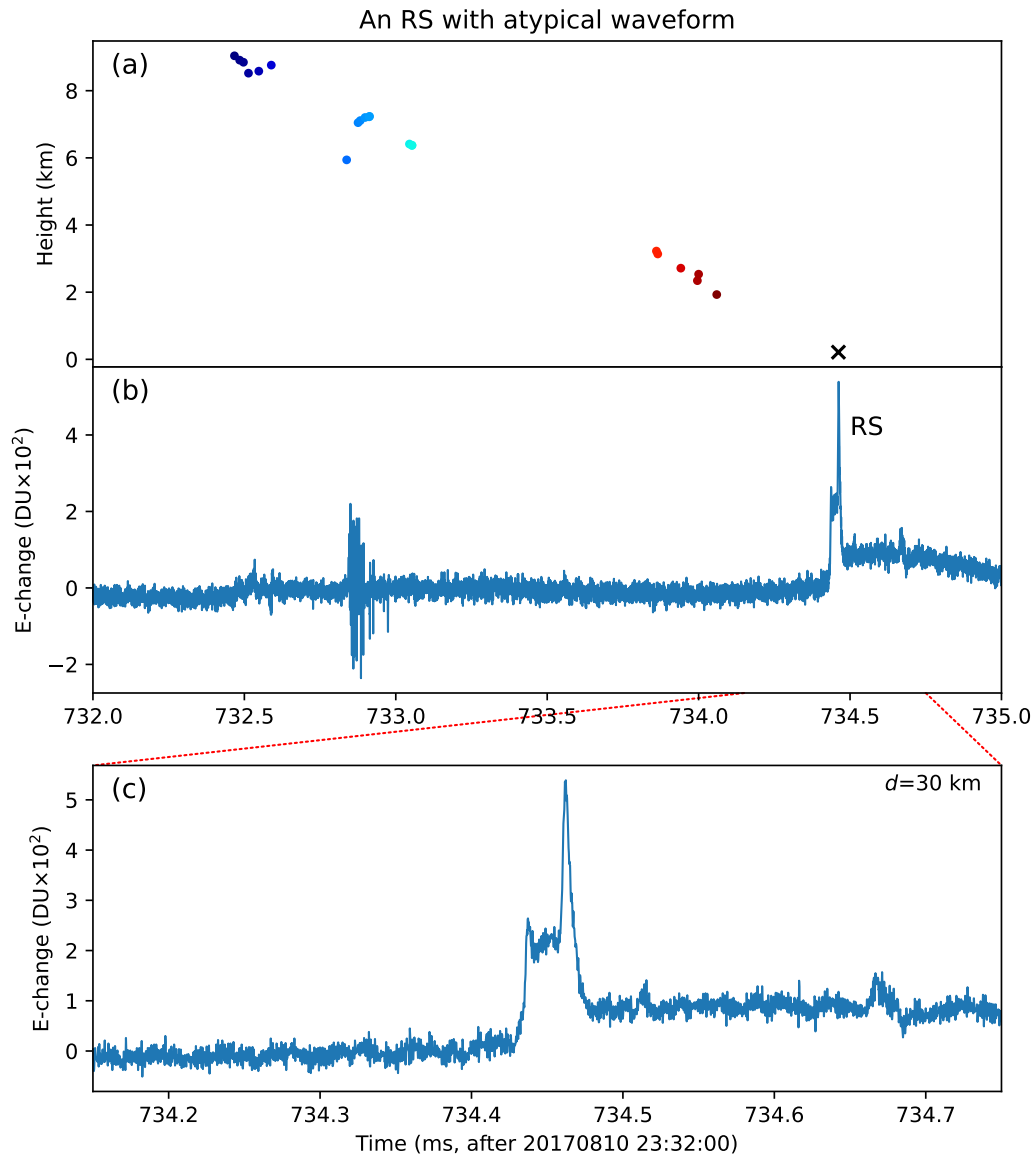


Figure 5. Location result and E-change waveforms of an RS misclassified as an IC discharge. (a) Height-time location results of the dart leader preceding the RS. The cross sign represents the RS. (b) E-change waveform of the RS and preceding discharges. (c) E-change waveform of the RS. The value of d represents the distance between the RS and the observation site recording the waveform.

404 We also manually located these pulses to make sure that there were no large errors in
405 the source height results. We can see that these pulses have relatively short rise times
406 and much longer fall times. Pulses in Figures 4e-g also have fine structures superimposed
407 on the falling part, similar to waveforms of first RSs, and the pulse in Figure 4h resembles
408 the waveform of a subsequent RS. These similar features as RS waveforms make it almost
409 impossible to correctly classify them as IC discharges without the 3-D location results.

410 Another example of an IC pulse appearing similar to RS pulses is shown in Figure 6
411 along with location results of preceding discharges. From the height-time location results
412 in Figure 6a, we can see that a leader first propagated above 6.5 km and then descended
413 to a height of about 5.5 km, and then the large IC pulse is produced, represented by the
414 cross sign. From the E-change waveform in Figure 6c, we can see that the large IC pulse
415 is very similar to an RS pulse, with preceding pulses resembling stepped leader pulses.
416 With the help of the 3-D location results, we can be sure that this RS-like pulse is produced
417 by IC discharges. We are not aware of any study reporting such RS-like IC pulses. In
418 our future studies, we will explore the mechanism responsible for these special IC pulses.

419 These examples of special RS and IC waveforms illustrate the fact that some RSs
420 and IC discharges produce atypical radiation waveforms from which the discharge types
421 cannot be accurately determined, resulting in a fundamental difficulty to achieve very
422 high accuracy and efficiency using only waveform information. This result also illustrates
423 the importance of accurate 3-D location results in scientific investigations of lightning
424 phenomena.

425 5 Conclusions

426 Using a large dataset with 3-D location results, we built a classifier for radiation
427 waveforms of negative RSs based on the Random Forest classifier. Eleven simple parameters
428 are defined for building the classifier, including three parameters related with pulse characteristics
429 and eight parameters related with relative strength of pulses. A classification accuracy
430 of 98.84% and an identification efficiency of 98.81% are achieved. We also demonstrated
431 methods to tune the tradeoff between the accuracy and the efficiency so the classifier can
432 be used in applications with different requirements of the accuracy or the efficiency. Although
433 the classifier is built based on the observation of a compact lightning mapping system,
434 we demonstrated that the classifier also has high accuracy and efficiency for remote lightning
435 discharges and can be readily used in long-baseline LLSs. With the same methods, we
436 also built a classifier for positive RSs which has similarly high accuracy and efficiency
437 as the classifier for negative RSs.

438 Misclassified RS and IC waveforms are examined and some common reasons for misclassifications
439 are analyzed. We demonstrated that RSs sometimes produce radiation waveforms that
440 are largely different from normal RS waveforms, and IC discharges sometimes produce
441 waveforms that appear very similar to RS waveforms. Therefore, some RS and IC waveforms
442 are fundamentally difficult to be correctly classified without 3-D location information,
443 and it is likely that such misclassifications commonly exist in most LLSs. The results
444 also imply the importance of 3-D location results in detailed analyses of lightning phenomena.

445 Open Research Section

446 Datasets for building and testing the classifiers as well as waveform figures of all
447 positive and negative RSs can be found at <https://doi.org/10.5281/zenodo.7641792>. Sample
448 Python scripts for using the classifiers will be made publicly available after the acceptance
449 of this paper.

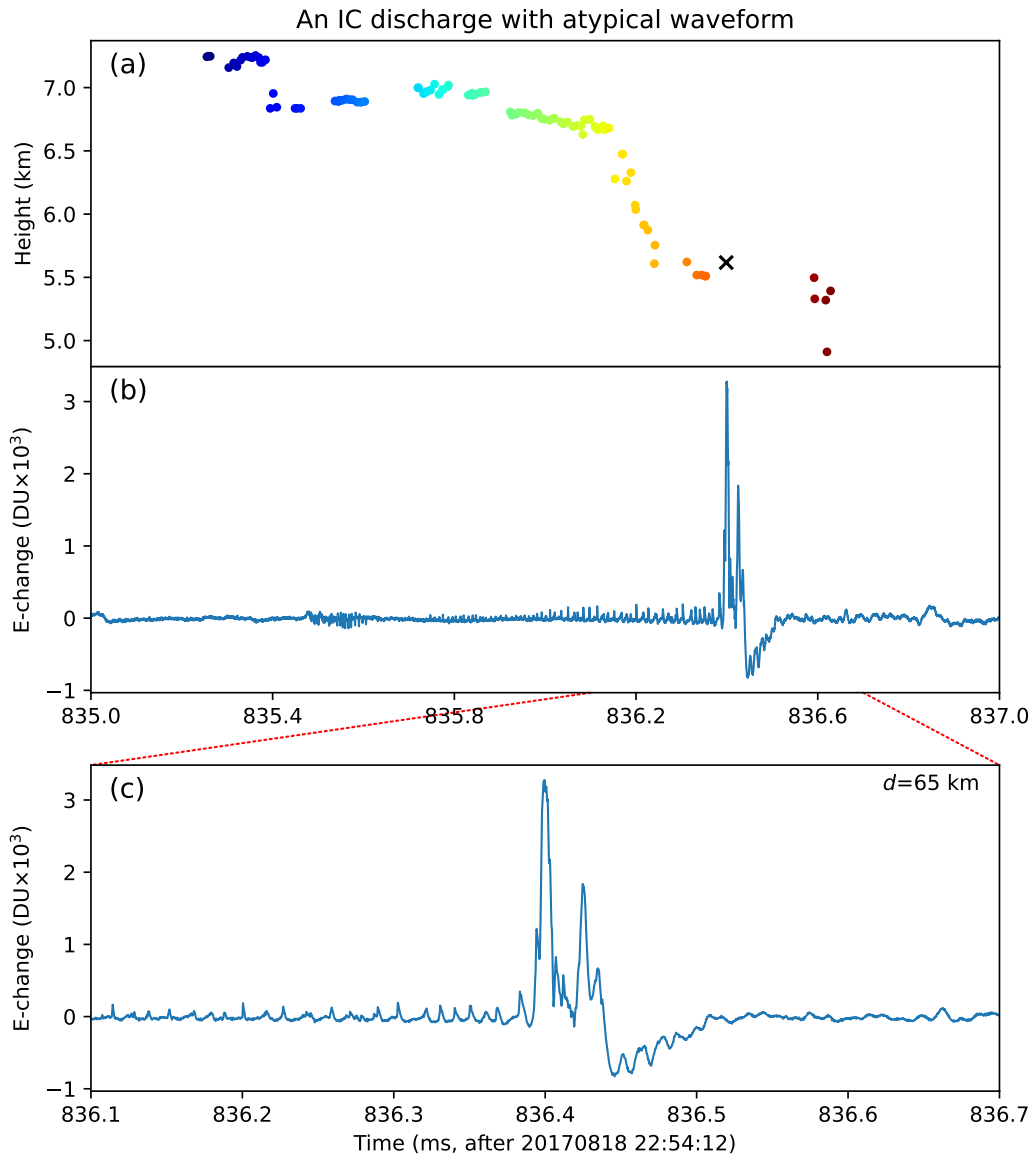


Figure 6. Location result and E-change waveforms of an IC pulse misclassified as an RS pulse. (a) Height-time location results of the IC pulse and preceding discharges. The cross sign represents the location of the IC pulse. (b) E-change waveform of the IC pulse and preceding discharges. (c) E-change waveform of the IC pulse. The value of d represents the distance between the IC discharge and the observation site recording the waveform.

450 **Acknowledgments**

451 This study was supported by the Ministry of Education, Culture, Sports, Science, and
 452 Technology of Japan (Grants 20H02129 and 21K03681).

453 **References**

- 454 Araki, S., Nasu, Y., Baba, Y., Rakov, V. A., Saito, M., & Miki, T. (2018, sep).
 455 3-d finite difference time domain simulation of lightning strikes to the 634-m
 456 tokyo skytree. *Geophysical Research Letters*, *45*(17), 9267–9274. doi:
 457 <https://doi.org/10.1029/2018gl078214>
- 458 Ballarotti, M. G., Saba, M. M. F., & Pinto, O. (2005). High-speed camera
 459 observations of negative ground flashes on a millisecond-scale. *Geophysical*
 460 *Research Letters*, *32*(23). doi: <https://doi.org/10.1029/2005gl023889>
- 461 Betz, H.-D., Schmidt, K., Oettinger, P., & Wirz, M. (2004, jun). Lightning
 462 detection with 3-d discrimination of intracloud and cloud-to-ground discharges.
 463 *Geophysical Research Letters*, *31*(11), n/a–n/a. doi: 10.1029/2004gl019821
- 464 Cai, L., Liu, W., Zhou, M., Wang, J., Yan, R., Tian, R., & Fan, Y. (2022, dec).
 465 Differences of electric field parameters for lightning strikes on tall towers and
 466 nonelevated objects. *IEEE Transactions on Electromagnetic Compatibility*,
 467 *64*(6), 2113–2121. doi: <https://doi.org/10.1109/temc.2022.3207237>
- 468 Cummins, K. L., & Murphy, M. J. (2009, aug). An overview of lightning locating
 469 systems: History, techniques, and data uses, with an in-depth look at the u.s.
 470 NLDN. *IEEE Transactions on Electromagnetic Compatibility*, *51*(3), 499–518.
 471 doi: <https://doi.org/10.1109/temc.2009.2023450>
- 472 Fleenor, S. A., Biagi, C. J., Cummins, K. L., Krider, E. P., & Shao, X.-M.
 473 (2009, feb). Characteristics of cloud-to-ground lightning in warm-season
 474 thunderstorms in the central great plains. *Atmospheric Research*, *91*(2-4),
 475 333–352. doi: <https://doi.org/10.1016/j.atmosres.2008.08.011>
- 476 Kohlmann, H., Schulz, W., & Pedebay, S. (2017, oct). Evaluation of EUCLID
 477 IC/CG classification performance based on ground-truth data. In *2017*
 478 *international symposium on lightning protection (XIV SIPDA)*. IEEE. doi:
 479 <https://doi.org/10.1109/sipda.2017.8116896>
- 480 Kong, X., Qie, X., Zhao, Y., & Zhang, T. (2009, feb). Characteristics of
 481 negative lightning flashes presenting multiple-ground terminations on a
 482 millisecond-scale. *Atmospheric Research*, *91*(2-4), 381–386. doi: <https://doi.org/10.1016/j.atmosres.2008.03.025>
- 483 Leal, A. F., Rakov, V. A., & Rocha, B. R. (2019, aug). Compact intracloud
 484 discharges: New classification of field waveforms and identification by lightning
 485 locating systems. *Electric Power Systems Research*, *173*, 251–262. doi:
 486 <https://doi.org/10.1016/j.epsr.2019.04.016>
- 487 Lin, Y. T., Uman, M. A., Tiller, J. A., Brantley, R. D., Beasley, W. H., Krider,
 488 E. P., & Weidman, C. D. (1979). Characterization of lightning return stroke
 489 electric and magnetic fields from simultaneous two-station measurements.
 490 *Journal of Geophysical Research*, *84*(C10), 6307. doi: <https://doi.org/10.1029/jc084ic10p06307>
- 491 Paul, C., Heidler, F. H., & Schulz, W. (2020, feb). Performance of the european
 492 lightning detection network EUCLID in case of various types of current
 493 pulses from upward lightning measured at the peissenberg tower. *IEEE*
 494 *Transactions on Electromagnetic Compatibility*, *62*(1), 116–123. doi:
 495 <https://doi.org/10.1109/temc.2019.2891898>
- 496 Pavanello, D., Rachidi, F., Janischewskyj, W., Rubinstein, M., Hussein, A. M.,
 497 Petrache, E., ... Jaquier, A. (2007, jul). On return stroke currents and remote
 498 electromagnetic fields associated with lightning strikes to tall structures:
 499 2. experiment and model validation. *Journal of Geophysical Research:*
 500 *Atmospheres*, *112*(D13). doi: <https://doi.org/10.1029/2006jd007959>

- 503 Rison, W., Thomas, R. J., Krehbiel, P. R., Hamlin, T., & Harlin, J. (1999, dec). A
 504 GPS-based three-dimensional lightning mapping system: Initial observations
 505 in central new mexico. *Geophysical Research Letters*, *26*(23), 3573–3576. doi:
 506 <https://doi.org/10.1029/1999gl010856>
- 507 Schulz, W., Diendorfer, G., Pedeboy, S., & Poelman, D. R. (2016, mar). The
 508 european lightning location system EUCLID – part 1: Performance analysis
 509 and validation. *Natural Hazards and Earth System Sciences*, *16*(2), 595–605.
 510 doi: <https://doi.org/10.5194/nhess-16-595-2016>
- 511 Sun, Z., Qie, X., Liu, M., Jiang, R., Wang, Z., & Zhang, H. (2016, jan).
 512 Characteristics of a negative lightning with multiple-ground terminations
 513 observed by a VHF lightning location system. *Journal of Geophysical*
 514 *Research: Atmospheres*, *121*(1), 413–426. doi: [https://doi.org/10.1002/](https://doi.org/10.1002/2015jd023702)
 515 [2015jd023702](https://doi.org/10.1002/2015jd023702)
- 516 Thottappillil, R., Rakov, V. A., & Uman, M. A. (1997, mar). Distribution of charge
 517 along the lightning channel: Relation to remote electric and magnetic fields
 518 and to return-stroke models. *Journal of Geophysical Research: Atmospheres*,
 519 *102*(D6), 6987–7006. doi: <https://doi.org/10.1029/96jd03344>
- 520 Wang, J., Huang, Q., Ma, Q., Chang, S., He, J., Wang, H., . . . Gao, C. (2020, feb).
 521 Classification of VLF/LF lightning signals using sensors and deep learning
 522 methods. *Sensors*, *20*(4), 1030. doi: <https://doi.org/10.3390/s20041030>
- 523 Wu, T., Wang, D., Huang, H., & Takagi, N. (2021, nov). The strongest negative
 524 lightning strokes in winter thunderstorms in japan. *Geophysical Research*
 525 *Letters*, *48*(21). doi: <https://doi.org/10.1029/2021gl095525>
- 526 Wu, T., Wang, D., & Takagi, N. (2018a, apr). Lightning mapping with an array of
 527 fast antennas. *Geophysical Research Letters*, *45*(8), 3698–3705. doi: [https://](https://doi.org/10.1002/2018gl077628)
 528 doi.org/10.1002/2018gl077628
- 529 Wu, T., Wang, D., & Takagi, N. (2018b, aug). Locating preliminary breakdown
 530 pulses in positive cloud-to-ground lightning. *Journal of Geophysical Research:*
 531 *Atmospheres*. doi: <https://doi.org/10.1029/2018jd028716>
- 532 Wu, T., Wang, D., & Takagi, N. (2019, sep). Velocities of positive leaders
 533 in intracloud and negative cloud-to-ground lightning flashes. *Journal*
 534 *of Geophysical Research: Atmospheres*, *124*(17-18), 9983–9995. doi:
 535 <https://doi.org/10.1029/2019jd030783>
- 536 Wu, T., Wang, D., & Takagi, N. (2021, aug). Compact lightning strokes in winter
 537 thunderstorms. *Journal of Geophysical Research: Atmospheres*, *126*(15). doi:
 538 <https://doi.org/10.1029/2021jd034932>
- 539 Wu, T., Wang, D., & Takagi, N. (2022, nov). On the intensity of first return
 540 strokes in positive cloud-to-ground lightning in winter. *Journal of Geophysical*
 541 *Research: Atmospheres*, *127*(22). doi: <https://doi.org/10.1029/2022jd037282>
- 542 Zhu, Y., Bitzer, P., Rakov, V., & Ding, Z. (2021, jan). A machine-learning approach
 543 to classify cloud-to-ground and intracloud lightning. *Geophysical Research*
 544 *Letters*, *48*(1). doi: <https://doi.org/10.1029/2020gl091148>
- 545 Zhu, Y., Rakov, V. A., Tran, M. D., Lyu, W., & Micu, D. D. (2018, sep). A
 546 modeling study of narrow electric field signatures produced by lightning strikes
 547 to tall towers. *Journal of Geophysical Research: Atmospheres*, *123*(18). doi:
 548 <https://doi.org/10.1029/2018jd028916>
- 549 Zhu, Y., Rakov, V. A., Tran, M. D., & Nag, A. (2016, dec). A study of national
 550 lightning detection network responses to natural lightning based on ground
 551 truth data acquired at LOG with emphasis on cloud discharge activity.
 552 *Journal of Geophysical Research: Atmospheres*, *121*(24), 14,651–14,660. doi:
 553 <https://doi.org/10.1002/2016jd025574>
- 554 Zhu, Y., Stock, M., Lapierre, J., & DiGangi, E. (2022, may). Upgrades of the earth
 555 networks total lightning network in 2021. *Remote Sensing*, *14*(9), 2209. doi:
 556 <https://doi.org/10.3390/rs14092209>